J Mater Sci (2007) 42:5470–5475
DOI 10.1007/s10853-006-0983-x

Electrical conduction and relaxation mechanism in $Li_2AlZr[PO_4]_3$

T. Savitha · S. Selvasekarapandian · C. S. Ramya · M. S. Bhuvaneswari · P. C. Angelo

Received: 5 April 2006 / Accepted: 21 September 2006 / Published online: 3 April 2007

Abstract Li-ion electrolyte NASICON type $Li_2AlZr[PO_4]_3$ has been prepared by Solid State Reaction method. Formation of the sample has been confirmed by XRD and TGA–DTA analysis. Electrical conductivity studies have been performed in the frequency range 42 Hz–5 MHz within the temperature range 523–623 K using aluminium as blocking electrodes. The conductivity has been found to be 1×10^{-5} S cm^{-1} at 623 K. Dielectric spectra show the decrease in dielectric constant with increase in frequency. Dielectric loss spectra reveal that dc conduction contribution predominates in the sample. Spectroscopic plots of complex modulus suggest the Non-Debye behaviour of the electrical relaxation within the temperature range studied.

Introduction

Lithium ion conductors constitute a very important class of solid electrolyte in solid state batteries because of the high chemical activity of Li^+ ions. Li-ion conducting NASICON type compounds have been extensively studied because they exhibit unique property such as low sintering temperature, three dimensional framework holding easy conduction pathways resulting in high ionic conductivity [1]. Lithium titanium phosphate material based on the above framework consist of $[PO_4]$ tetrahedral connected in corner sharing arrangement with $[TiO_6]$ octrahedra [2]. But the conductivity of this material is not good enough for practical applications. Many researchers reported that the partial substitution of Ti^{4+} with trivalent cations such as In^{3+}, Sc^{3+}, Al^{3+} [2, 3] etc enhances the conductivity. Among these substitutions Al^{3+} substitution provides improvements in density and sinterability resulting in high Li ion conductivity and air stability of LATP. It has been postulated that Lithium loss during sintering at high temperatures causes a significant reduction in the conductivity of undoped $LiTi(PO_4)_3$ as significant weight losses above 1100 °C are observed by thermogravimetric analysis. The Al-doped materials form dense ceramics more readily and are, therefore, less likely to lose Lithia [4]. The improvement in densification may be associated with extra intergranular low melting or glassy phases which can act as fluxes to improve sinterability and conductivity. The bulk ionic conductivity of LATP was reported to be 7×10^{-4} S cm^{-1} at 25 °C.

But the reduction of Ti^{4+} to Ti^{3+} with Li metal restricts their use as solid electrolytes in battery applications resulting in instability [5]. Robertson et al., reported that Ge and Hf ($\sigma = 1 \times 10^{-4}$ S cm^{-1} at 25 °C) replacement in the place of Ti results in stability towards lithium but are significantly more costly to produce [4]. Thus in the present study, Ti has been replaced with Zr to form $Li_2AlZr[PO_4]_3$. Dielectric and modulus analysis have been done to study the conduction and relaxation mechanism of the sample using Impedance analyzer.

Experimental

The compound $Li_2AlZr[PO_4]_3$ has been prepared by Solid State Reaction method. The raw materials used are Li_2CO_3, $(NH_4)_2HPO_4$, ZrO_2 and Al_2O_3. One of the raw materials

T. Savitha · S. Selvasekarapandian (✉) ·
C. S. Ramya · M. S. Bhuvaneswari
Solid State and Radiation Physics Laboratory, Department of Physics, Bharathiar University, Coimbatore 641 046, India
e-mail: sekarapandian@yahoo.com

P. C. Angelo
Department of Metallurgical Engineering, P.S.G. College of Technology, Coimbatore 641 004, India

ZrO_2 has been prepared by co-precipitation method [6]. The reagents are taken in stoichiometric ratio and ground using a mortar and a pestle. The homogenized powder has been heated to 850 °C and kept for 2 h at this temperature. TGA–DTA measurements has been taken using STA-1500 thermal analyzer with a resolution of 0.01 mg. The mixture of raw materials has been kept in a crucible and heated from room temperature to 700 °C at a rate of 5 °C per minute. X-ray diffractogram (XRD) has been taken to confirm the formation of samples with desired phase, by using Philips X-ray diffractometer PW 1830. The resultant sample is crushed into fine powder and spread in a die, to which a pressure of 4000 kg cm^{-2} is applied to form pellet with 1 mm thickness and 1.0 cm diameter. The pellet has been sintered at 450 °C for 2 h. The dielectric measurements are performed by placing the pellet in between two aluminium blocking electrodes within the frequency range 42 Hz to 5 MHz from 523 to 623 K using a computer controlled HIOKI 3532 LCR meter.

Results and discussion

TGA–DTA analysis

Figure 1 shows the TGA–DTA curves of the mixture of raw materials with heating rate of 5 °C per minute from room temperature up to 700 °C. TGA curves show three regions of weight loss. The thermogravimetric curves of the mixtures showed a weight loss over the temperature range from ambient to 155 °C (Ist region) which corresponds to the elimination of superficial water adsorbed on the sample. The second weight loss in the temperature range 155–333 °C may be attributed to the decomposition of $(NH_4)_2HPO_4$ with the evolution of NH_3. The third region corresponds to the decomposition of Li_2CO_3 with a weight loss of about 3%. At higher temperatures the chemical reaction that take place do not lead to any weight loss, as shown in TGA curve. In the DTA curve the two endothermic peaks at 148 and 184 °C can be attributed to the decomposition of $(NH_4)_2HPO_4$ which melts at 155 °C with ammonia evolution. The exothermic effect at 374°C can be probably related to the decomposition of Li_2CO_3 to Li_2O followed by the formation of the sample [7].

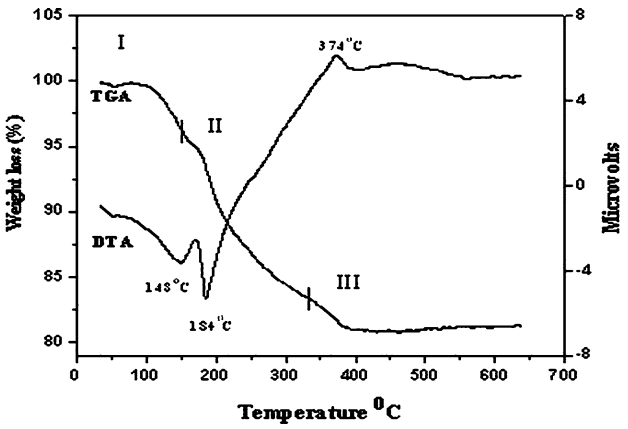

Fig. 1 TGA–DTA curves of the sample with heating rate of 5 °C per minute

XRD analysis

The X-ray diffraction pattern of the sample has been taken using X-ray diffractometer with Cu K_α radiation having a wavelength of 1.5417 Å. The XRD pattern of $Li_2AlZr[PO_4]_3$ is shown in Fig. 2. The three strong intensity peaks at 2θ = 23.3749, 20.0917 and 19.6228 indicate the formation of the sample. Some traces of ZrO_2, Al_2O_3 have been observed in the XRD pattern. Peak at 2θ = 13.992 corresponding to the secondary phase, Lithium Zirconium Phosphate (JCPDF 44-0010) has also been observed. Thus the pattern reveals the polycrystalline nature of the sample. The particle size (D) has been estimated using the Debye Scherrer's formula,

$$D = \frac{0.94\lambda}{\beta_{2\theta}\cos\theta} \quad (1)$$

where, λ is the wavelength of the X-ray and $\beta_{2\theta}$ is the full width at half maximum of the corresponding peak of the XRD pattern. The particle size for the sample is in the order of 38 nm. This confirms the formation of nano crystalline phases in the present sample.

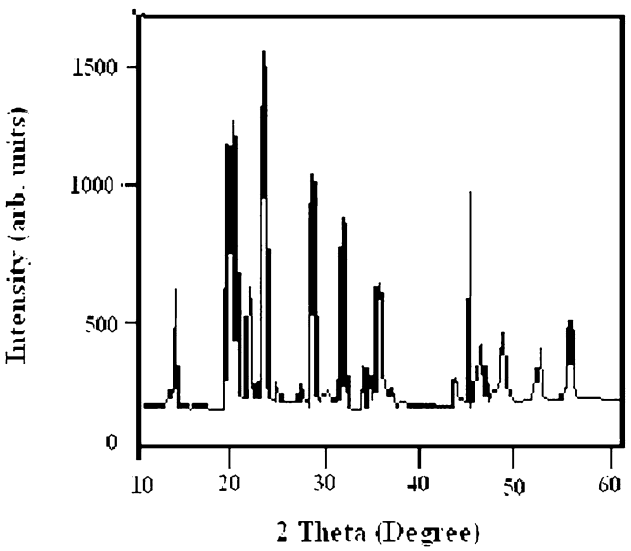

Fig. 2 XRD pattern of $Li_2AlZr[PO_4]_3$

Conductivity analysis

The conductivity has been found to vary linearly with temperature obeying Arrhenius relation given by,

$$\sigma_b = \sigma_0 \text{ Exp } (- E_a/kT) \quad (2)$$

where σ_0 is pre-exponential factor and k is the Boltzmann constant, T is the absolute temperature and E_a is the activation energy for the migration of Li^+ ions. The dc activation energy calculated from the slope of the straight line (Fig. 3) has been found to be 0.83 eV in the temperature range studied. The dc conductivity of the sample has been found to be 1×10^{-5} S cm^{-1} at 623 K.

Dielectric analysis

The frequency dependence of the dielectric function $\varepsilon(\omega)$ of a solid reflects the dynamic response of the constituents of the solid. The complex permittivity is given by

$$\varepsilon_r = \varepsilon' - i\varepsilon'' \quad (3)$$

where ε' is the real part of complex permittivity or dielectric constant and ε'' is the dielectric loss. Figure 4a shows that the real part of the dielectric permittivity decreases with increase in frequency. At low frequencies due to space charge accumulation a gradual increase in the dielectric constant has been observed. At higher frequencies the change in the direction of the electric field lines is too fast to be followed by the charged ions and hence the dielectric constant decreases. The plot of Log ε'' vs Logω is shown in Fig. 4b. The slope of the straight line has been found to be in the range of –0.7 to –0.9. Dissipation (loss) factor tanδ is given by

$$\tan\delta = \sigma_{dc}/\omega\varepsilon \quad (4)$$

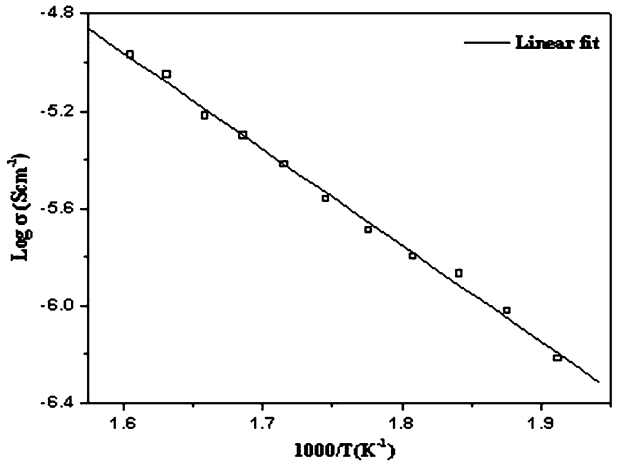

Fig. 3 Arrhenius plot of $Li_2AlZr[PO_4]_3$

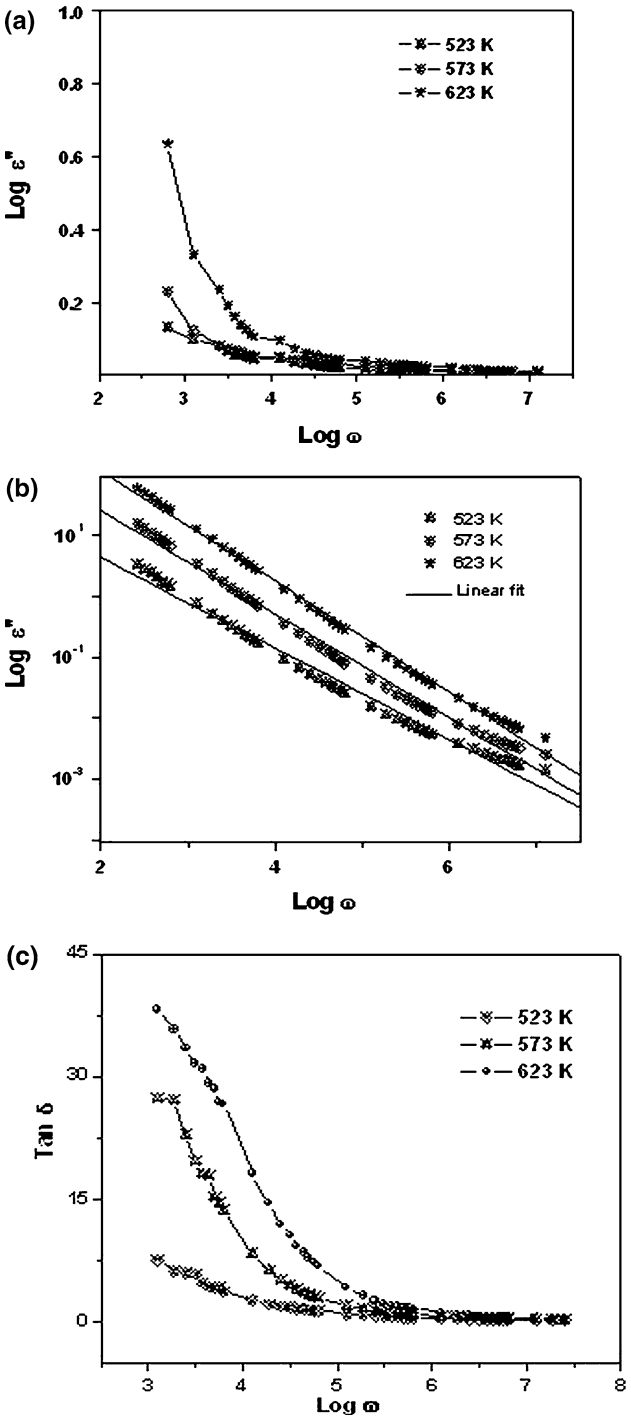

Fig. 4 Dielectric spectra of $Li_2AlZr[PO_4]_3$. (**a**) Real part of dielectric constant vs Logω; (**b**) Imaginary part of dielectric constant vs Logω; (**c**) Frequency dependent loss factor

which can be rewritten as

$$\varepsilon'' = \sigma_{dc}/\omega$$

since

$$\tan\delta = \varepsilon''/\varepsilon' \quad (5)$$

Hence log ε'' vs log ω plot with a slope value near to –1 indicates that the dc conduction contribution is predominant in the present sample. The absence of peak in the dielectric loss spectra also indicates the long-range ionic conductivity dominance in dielectric response at low frequencies [8]. The deviation from the unity may be attributed to the space charge effects at low frequencies. Figure 4c shows the frequency dependence of tan δ at various temperatures. The absence of any loss peak within the temperature range studied reveals that hopping of charge carriers dominates both the polarization and relaxation phenomenon [9]. This frequency dispersion due to the charge carrier system can be correlated to the distribution of relaxation times. From the Fig. 4(a, b, c) it is understood that ε', ε'' and tan δ increase with temperature. The increase in the dielectric constant may be attributed to the migration and polarization of Li^+ ions [10]. Thus the dielectric dispersion observed with temperature and frequency variation confirms the electrical charge hopping mechanism which governs both the charge transport and relaxation phenomenon in the present sample.

Modulus analysis

In electrical modulus spectra electrode polarization effects are suppressed and thus it mainly reflects the bulk electrical properties of the sample. The complex modulus is given by the inverse of complex dielectric permittivity

$$M^* = 1/\varepsilon^* = M' + iM'' \quad (6)$$

Figure 5 shows the spectroscopic plots of M′ and M″. At low frequency region M′ value tends towards zero, which suggest that electrode polarization is negligible. M″(ω) vs Log ω (Fig. 5b) shows single asymmetric peak in the temperature range studied indicating the non-exponential decay of the electric field in response to the applied field. The low frequency part of the peak indicates the long-range motion of the mobile ions and the high frequency side of the peak indicates the confined motion of the ions within a potential well. The amplitude of the peak does not remain constant within the temperature range studied which reveals the distribution of relaxation time [11]. The shift in the peak frequencies and the variation of the maximum (M''_{max}) indicate the variation of capacitance with increase in temperature. The same behaviour has been observed by Nobre et al., in the ceramic $Na_{1-x}K_xNbO_3$ [12]. This behaviour also suggests that the dielectric relaxation is activated thermally in which hopping process of charge carriers are dominating. The bulk capacitance values has been calculated using the relation $M''_{max} = C_0/2C_b$ (Table 1), where C_0 is the vacuum capacitance of the

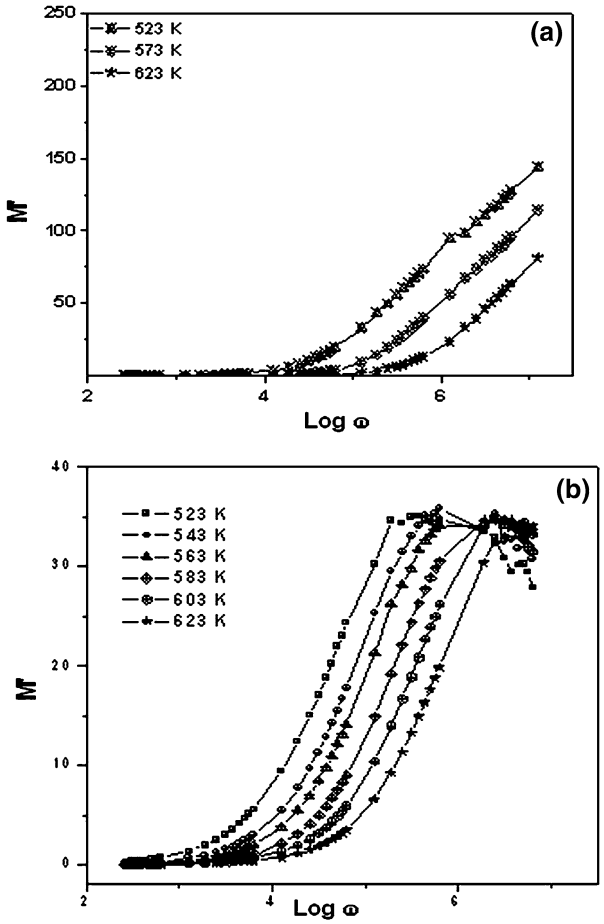

Fig. 5 Modulus spectra of $Li_2AlZr[PO_4]_3$ for different temperatures. (**a**) Real part of modulus vs Logω; (**b**) Imaginary part of modulus vs Logω

cell and they are found to be in the order of pF revealing the bulk relaxation in the sample. The frequency dependence of modulus has been described by stretched KWW relaxation function ϕ(t), which describes the electric field decay [13],

$$M*(\omega) = \frac{1}{\varepsilon_\infty}\left[1 - \int_0^\infty \frac{d\phi}{dt} e_{-j\omega t} dt\right] \quad (7)$$

Table 1 Relaxation parameters calculated from Modulus spectra

Temperature (K)	β	C_b (F)	τ (s)
523	0.33	3.3×10^{-11}	1×10^{-6}
543	0.41	3.5×10^{-11}	9×10^{-7}
563	0.45	3.6×10^{-11}	7×10^{-7}
583	0.5	3.8×10^{-11}	5×10^{-7}
603	0.56	4×10^{-11}	3×10^{-7}
623	0.61	4.2×10^{-11}	2×10^{-7}

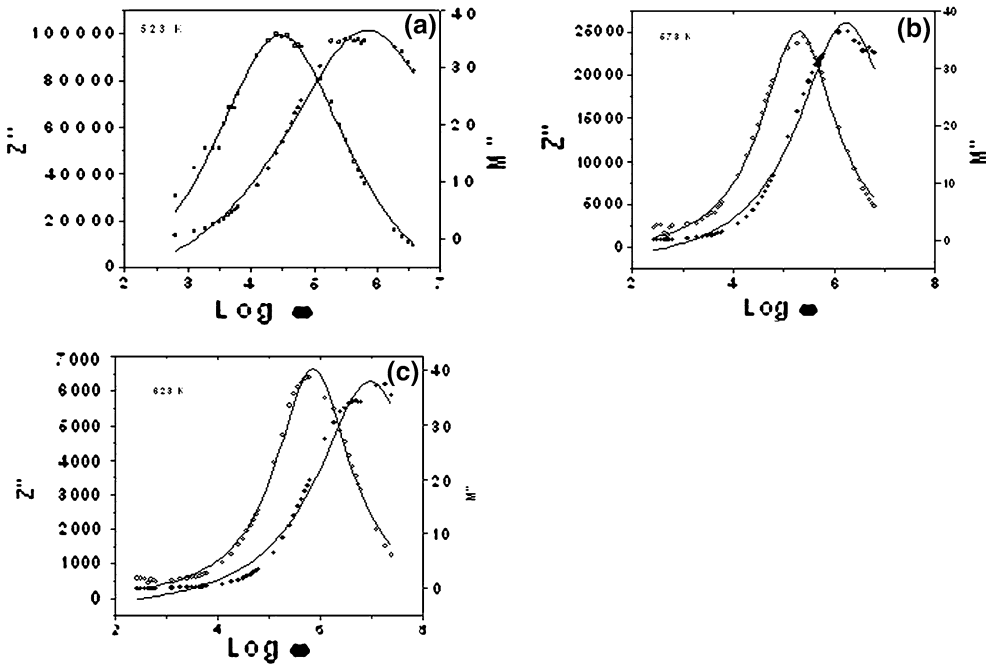

Fig. 6 Combined spectroscopic plots of Z″ (ω) & M″(ω) of $Li_2AlZr[PO_4]_3$ at (**a**)523 K, (**b**) 573 K, (**c**) 623 K

Kohlarusch-Williams-Watts (KWW) function is given by,

$$\phi(t) = \exp(-t/\tau_0)^{\beta} \quad (8)$$

where τ_0 is the time at which $\phi(t)$ decays to 1/e and the exponent β describes the breadth of the distribution in the limits of $0 \leq \beta \leq 1$. The non-exponential character of the electric field decay and the corresponding frequency dispersion in the dielectric constant are a result of the microscopic heterogeneity of the system. Stretching parameter β has been calculated by extracting FWHM of the modulus peak using $\beta = 1.14/\text{FWHM}$ and is given in Table 1.

In order to investigate the electrical microstructures of the pellet, the experimental data were re-plotted as imaginary parts of the impedance, Z″ vs electric modulus, M″, against log frequency. The combined spectroscopic plots of Z″(ω) & M″(ω) becomes important since impedance plots highlights the most resistive element of the sample and modulus plot highlights the capacitive element which explains conduction mechanism within the grain interior [14]. Figure 6(a–c) shows the combined spectroscopic plots of Z″(ω) & M″(ω) for 523, 573 & 623 K. The polarization peaks of Z″(ω) & M″(ω) do not coincide and they are separated by one decade which again confirms the distribution of relaxation time in the present sample. This small difference in the peak frequency is common phenomena associated with dispersions in bulk ac conductivity and dielectric permittivity of a non-ideal dispersive conductor [15]. The width of the peaks of both Z″(ω) & M″(ω) are greater than Debye peak (1.14 decades) suggesting the non-debye type relaxation for all the temperatures. Both Z″(ω) & M″(ω) peaks shifts towards higher frequencies with increase in temperature and the peak frequency can be correlated to average electrical conductivity relaxation time ($\tau = 1/2\pi f_p$). Relaxation time calculated has been found to be decreased with increase in temperature (Table 1).

Conclusion

Lithium ion conducting electrolyte $Li_2AlZr[PO_4]_3$ has been prepared by Solid State Reaction method and conductivity analysis has been performed. TGA–DTA analysis and XRD spectrum confirm the formation of the sample. The conductivity has been found to be 1×10^{-5} S cm^{-1} at 623 K. The activation energy calculated from the Arrhenius plot has been found to be 0.83 eV. Dielectric constant decreases with increase in frequency due to the high periodic reversal of the applied field. Dielectric loss spectra show straight lines with slope in the range –0.7 to –0.9 which reveals the contribution of dc conduction mechanism. The increase of dielectric functions with temperature suggests the contribution of migration polarization of Li^+ ions. Imaginary part of modulus shows asymmetric peaks with β in the range 0.33–0.61. Relaxation time calculated from the peak frequency has been found to decrease, within the temperature studied.

References

1. Kang H-B, Cho N-H (1999) J Mater Sci 34:5005; DOI: 10.1023/A: 1004784327302
2. Wong S, Newman PJ, Best AS (1998) J Mater Chem 8(10):2199

3. Yoshikawa K, Hayakawa N, Suzuki T (1999) J Eur Cermaic Soc 19:879
4. Robertson AD, West AR, Ritchie AG (1997) Solid State Ionics 104:1
5. Thangadurai V, Shukla AK, Gopalakrishnan J (1999) J Mater Chem 9:739
6. Vijayakumar M, Selvasekarapandian S, Bhuvaneswari MS, HiranKumar G, Ramprasad G, Subramanian R, Angelo PC (2003) Physica B 334:390
7. Bauer EM, Bellitto C, Pasquali M, Prosini PP, Righinia G (2004) Electrochem Solid-State Lett 7(4):A85
8. Bohnke O, Emery J, Fourquet J-L (2003) Solid State Ionics 158:119
9. Bharadwaja SSN, Krupanidhi SB (2001) Thin Solid Films 391:126
10. Orliukas A, Dindune A, Kanepe Z (2003) Solid State Ionics 157:177
11. Ganuli M, Harish Bhat M, Rao KJ (1999) Solid State Ionics 122:23
12. Nobre MAL, Lanfredi S (2003) Catal Today 78:529
13. Melnikov P, Leon C, Santamaria J, Sanchez-Quesada F (1997) J Alloys Compounds 250:520
14. Sinclair DC, West AR (1988) J Mater Sci Lett 7:823
15. Almond DA, West AR (1983) Solid State Ionics 11:57